Folding the Carpenter's Tape: Boundary Layer Effects

C R Calladine and K A Seffen

Department of Engineering, University of Cambridge, Trumpington Street, Cambridge, CB2 1PZ.

kas14@cam.ac.uk

Abstract

The "carpenter's measuring tape" is a thin spring-steel strip, pre-formed to a curved cross-section of radius R, and which is straight when being used for measuring. Under bending moments it forms a localised hinge, in which the transverse curvature is suppressed, and the longitudinal radius, r, is approximately equal to R. F P J Rimrott made a simple strain-energy analysis of the hinge region for isotropic material, which predicted that $r = R$. Experimental observations and finite element computations both show that $\xi = r/R > 1$, where the value of ξ exceeds unity by up to 15%, depending on whether the tape is bent in "equal-sense" or "opposite-sense" curvature; and ξ varies linearly with Poisson's ratio in both cases. We make a minor change to Rimrott's analysis by introducing a *boundary layer*, in order better to satisfy the physical conditions at the free edges; and this successfully accounts for the observed behaviour of the tape.

Keywords: measuring tape; folded hinge; strip curvature; shell boundary layer

1 Introduction

The "carpenter's measuring tape" is a familiar household object. It is a thin spring-steel strip which, when extended in its relaxed state, is held straight by the fact that it has distinct transverse curvature, and can act as a slender beam. When it is coiled up into its capsule, this transverse curvature is suppressed, and the tape is in a state of high elastic strain energy.

When a straight portion of tape is bent, or its ends are brought closer together, the tape responds by forming a localised "hinge", in which the natural transverse curvature is suppressed, and its state is similar to that within the coiled-up tape.

Soon after these measuring-tapes were introduced—in the 1920s—G T Bennett, known for "the Bennett linkage" [1], pointed out to A E H Love, the celebrated elastician [2], that the radius of the localised hinge

was equal to the transverse radius of curvature of the relaxed, straight tape [3].

Almost certainly Bennett would also have pointed out that the hinge radius remained constant as the angle (ψ) of the hinge was varied, so that the tape existed in two distinct states—straight and hinged—, apart from two specific "transition regions" between them; and indeed that the radius of curvature of the hinge was the same whether the bending was "equal sense" (ES) or "opposite sense"(OS) [4], as is shown schematically in Fig. 1. Alas, Love did not provide an explanation of this remarkable phenomenon.

A simple and convincing explanation of Bennett's observation, by means of a strain-energy analysis, was eventually provided by F P J Rimrott, in 1970 [5]. That work also showed why the result did not depend on the value of Poisson's ratio for the material, or on the angle of the bend, or on the direction of bending. We shall reproduce it below.

Seffen [6] showed, by means of experiment and finite element analysis, that the radius of the hinge actually tended to be somewhat larger than Rimrott's prediction—by as much as 15% in OS but less in ES bending. The aim of the present paper is to explain Seffen's observations by means of a relatively simple extension of Rimrott's analysis; and to confirm that the deviation from Rimrott's result depends significantly on the value of Poisson's ratio, ν, for the material.

The layout of the remainder of the paper is as follows. First we define the main variables of the problem. Next we reproduce Rimrott's analysis. Then we describe a simple modification of it in order to take account of the fact that it does not fully satisfy the physical boundary conditions along the free edges of the tape in the hinge region. Subsequent minimisation of the total strain energy of the system produces expressions for the increase of the radius of the hinge, which compare well with Seffen's results. We conclude the paper with a general discussion.

Notation

ES	equal-sense (bending)
OS	opposite-sense (bending)
b	width of tape (Fig. 1)
D	flexural stiffness of tape, $= Et^3/12(1-\nu^2)$
E	Young's modulus of elasticity for material
H	height of tape cross-section (Fig. 1)
L	length of tape
L^*	length of ploy region
$M_{x,y}$	bending-moment per unit length of tape, in x, y directions
M_0	edge moment applied to cylindrical shell (Fig. 2)
r	radius of longitudinal curvature in hinge region (Fig. 1)
R	radius of transverse curvature for relaxed, straight tape
t	thickness of tape
T	dimensionless characteristic group: $T = \alpha\sqrt{R/t}$
U	strain energy per unit area of hinge region
U_{T}	total strain energy of hinge according to Rimrott [5]
U_{R}	reduced total strain energy, according to our analysis
w	normal displacement of tape in hinge region
x	longitudinal surface coordinate in tape
y	transverse surface coordinate in tape: $y = 0$ at centre of tape

α angle (radians) subtended by tape's relaxed cross-section: $\alpha = b/R$ (Fig. 1)

γ dimensionless deviation of r from R: $\gamma = \xi - 1$

μ shell length parameter (Eqn 6)

ν Poisson's ratio for (isotropic) material

ξ dimensionless r: $\xi = r/R$

ϕ rotation of edge of shell under applied moment (Fig. 2)

χ_x longitudinal change of curvature in hinge region

χ_y transverse change of curvature in hinge region

ψ bend angle of hinge (Fig. 1)

2 Rimrott's Analysis

The unstressed cross-section of tape is taken to be a circular arc of thickness t, subtending angle α at radius R; the arc-width is $b = R\alpha$ and the height is $H = R(1 - \cos\alpha/2)$. Poisson's ratio for the isotropic material is ν and Young's modulus is E.

The tape is bent by equal and opposite moments applied to its long ends, which increase in magnitude until it buckles to form a localised folded hinge; see Fig. 1. The hinge is cylindrical, with a uniform longitudinal radius r independent of the fold angle, ψ, across the hinge. Whether the tape is bent in ES or OS, Fig. 1, Rimrott [5] determines $r = R$, in keeping with Bennett's remark.

Following Rimrott, we use orthogonal (x, y) surface coordinates in the tape: x lies along, and y is transverse to the tape; see Fig. 2. The changes in principal curvatures, χ, within the hinge region with respect to the straight, unstressed tape, are

$$\chi_x = \frac{1}{r} - 0 = \frac{1}{r}, \quad \chi_y = 0 - \left(\mp\frac{1}{R}\right) = \pm\frac{1}{R} \tag{1}$$

Here, and throughout the paper, the upper and lower signs (in $\mp$ or $\pm$) are for opposite-sense and equal-sense bending, respectively.

The deformed shape of the hinge is thus developable, and it stores strain energy only in bending. The transition in shape away from both sides of the hinge takes place over so-called "ploy" regions. These are practically straight, as shown schematically in Fig. 1; locally they have double curvature and non-zero in-plane strains, and consequently are much stiffer in bending than the hinge. These regions however do not vary in shape during bending; and thus they contribute no changes in stored energy, as the bending angle ψ increases.

The hinge radius, r, is therefore determined by the strain energy of bending in the hinge. The strain energy per unit area, U, is given by [7]

$$U = \frac{D}{2}\left[\chi_x^2 + \chi_y^2 + 2\nu\chi_x\chi_y\right] = \frac{D}{2}\left[\frac{1}{r^2} + \frac{1}{R^2} \pm \frac{2\nu}{Rr}\right] \tag{2}$$

Here D is the flexural rigidity of cross-section, equal to $Et^3/12(1-\nu^2)$.

The principal bending moments (per unit length) throughout the hinge are given by [7]

$$M_x = D\left[\chi_x + \nu\chi_y\right] = D\left[\frac{1}{r} \pm \frac{\nu}{R}\right], \quad M_y = D\left[\chi_y + \nu\chi_x\right] = D\left[\pm\frac{1}{R} + \frac{\nu}{r}\right] \tag{3}$$

and their positive senses are sketched in Fig. 2 for both senses of bending: note in particular the same senses of M_y along the curved edges—which should be obvious from how the natural transverse curvature becomes annulled.

The total strain energy, U_{T}, is found by multiplying U by the area of the hinge region, equal to $b \cdot r\psi$:

$$U_{\mathrm{T}} = \frac{b\psi D}{2}\left[\frac{1}{r} + \frac{r}{R^2} \pm \frac{2\nu}{R}\right] \tag{4}$$

The value of r is found by minimising U_{T} with respect to r. Thus

$$\frac{\mathrm{d}U_{\mathrm{T}}}{\mathrm{d}r} = 0 \quad \rightarrow \quad -\frac{1}{r^2} + \frac{1}{R^2} = 0 \tag{5}$$

i.e. $r = \pm R$, which is Rimrott's result. Note that the Poisson's ratio does not feature here; neither does the sense of bending, since ν appears only in the constant term of U_{T}.

3 Refined Analysis

An obvious anomaly in Rimrott's analysis is that, whilst there are non-zero bending moments M_y throughout the hinge region, and in particular at the curved edge—as shown in Figs 2(a,b)—the physical boundary condition at these free edges is clearly $M_y = 0$.

In order to present a more realistic picture of the behaviour of the tape in the vicinity of these edges of the hinge region, we have used finite element analysis to make a detailed study of the tape in the hinge region and the adjoining ploy regions for a particular case of OS bending. Specially small elements, numbering 201 across the tape width, for example, were used to capture the detailed properties.

Salient results are shown in Fig. 3; the caption indicates the parameters of the chosen case. Figure 3(a) shows the variation of M_y across the width of the tape. The blue curve corresponds to the middle of the hinge, and the red curve, inside the ploy region.

The form of M_y near the edges corresponds qualitatively to the response of a thin cylindrical shell to a uniform moment applied at its free edge (as in Fig. 2(c)), superposed onto the bending moments according to Rimrott's analysis (Figs 2(a,b)).

Over most of the tape's width $M_y = 1.28D/R$. On the assumption that Eqns 3 are still relevant, $R/r \approx 0.94$ for $\nu = 0.3$, giving r some 6% larger than in Rimrott's analysis.

The curve in Fig. 3(b) shows the profile of normal displacement, w, across the width of the tape in the hinge region, relative to a cylindrical surface of radius r. At the edges the displacement is a fraction of the tape's thickness. Again, this plot is consistent, locally, with the response of the shell loaded as in Fig. 2(c). In particular, the "edge perturbation" extends a distance of order $\sqrt{rt}$ into the shell, providing a "boundary layer".

Figure 3(c) shows the distributions of changes in curvature χ_x (blue) and χ_y (green) along the axial centre-line of the tape—in the x direction, over the hinge region and the adjoining ploy regions. The final hinge angle was set to π, with the ploy regions now parallel to each other. The uniform conditions in the hinge region are confirmed; there is also some complexity of the tape's behaviour in the ploy regions.

In order to remedy Rimrott's analysis, we now imagine a fictitious external agency applying steadily increasing counter-couples to the curved edges until the net moment there is reduced to zero.

For equal-sense bending, imposing an increasing clockwise couple on the near-side edge in Fig. 2(a), as in Fig. 2(c), will cause the edge to rotate clockwise, in proportion to the extra couple. The external work now done will be the integral of the net couple, which will be anti-clockwise and hence reducing, with respect to the increasing clockwise angle.

Strain energy will therefore be released in the process, which will form the correct boundary layer. The same argument applies also for the opposite-sense hinge, Fig. 3(b), but where the directions of counter-couple and edge rotation have switched.

The loss in strain energy is equal in magnitude to the strain energy that would be stored in a long, originally stress-free cylindrical shell of radius r and thickness t by a couple M_0 (say) uniformly imposed around the circumference, see Fig. 3(c). This is a classical problem in small displacement, linear elastic shell

theory [7] and one that is frequently adapted for tape analysis *e.g.* Seffen & Pellegrino [8], following the original treatment by Wuest [9], then later by Mansfield [10].

In particular, the rotation ϕ_0 of any generator at the loaded edge is linearly related to M_0 and given by [7]

$$\phi_0 = \mu M_0/D \quad \text{where} \quad \mu = (rt)^{1/2}/[3(1-\nu^2)]^{1/4} \tag{6}$$

This releases strain energy, u, per unit circumference of the boundary:

$$u = \phi_0 M_0/2 = \mu M_0^2/2D \tag{7}$$

We therefore propose to reduce Rimrott's U_{T} by the product of u and the total length of both free edges of hinge, $2r\psi$. Here, it is convenient to introduce ξ for dimensionless r as $\xi = r/R$; so Eqn 4 becomes

$$U_{\mathrm{T}} = \frac{b\psi D}{2R}\left[\frac{1}{\xi} + \xi \pm 2\nu\right] \tag{8}$$

This must now be reduced by $2r\psi \cdot \mu M_0^2/2D$.

M_0 is equivalent to M_y from Eqn 3:

$$M_0 = \frac{D}{R}\left[1 \pm \frac{\nu}{\xi}\right] \tag{9}$$

and the required reduction in strain energy becomes, after substituting for μ from Eqn 6, and re-arranging:

$$\frac{r\psi\mu}{D}\cdot\frac{D^2}{R^2}\left[1 + \frac{\nu^2}{\xi^2} \pm \frac{2\nu}{\xi}\right] = \frac{b\psi D}{2R}\cdot\frac{2(Rt)^{1/2}}{[3(1-\nu^2)]^{1/4}}\cdot\frac{1}{b}\left[\xi^{3/2} + \frac{\nu^2}{\xi^{1/2}} \pm 2\nu\xi^{1/2}\right] \tag{10}$$

We now introduce a constant, A, such that

$$A = \frac{2(Rt)^{1/2}}{[3(1-\nu^2)]^{1/4}}\cdot\frac{1}{b} = \frac{2}{[3(1-\nu^2)]^{1/4}}\cdot\frac{1}{\alpha}\cdot\sqrt{\frac{t}{R}} \tag{11}$$

Hence our final expression for the reduced strain energy, U_{R}, is

$$U_{\mathrm{R}} = \frac{b\psi D}{2R}\left[\frac{1}{\xi} + \xi \pm 2\nu - A\left(\xi^{3/2} + \frac{\nu^2}{\xi^{1/2}} \pm 2\nu\xi^{1/2}\right)\right] \tag{12}$$

Our boundary-layer modification of Rimrott's formula thus involves three terms, with ξ raised to powers of +3/2, -1/2, +1/2, respectively. The factor of 1/2 enters here because the width of the boundary layer is proportional to $\sqrt{rt}$.

Our task is now to minimise U_{R} with respect to ξ by setting $\mathrm{d}U_{\mathrm{R}}/\mathrm{d}\xi = 0$. This yields:

$$1 - \frac{1}{\xi^2} - \frac{A}{2}\left[3\xi^{1/2} - \frac{\nu^2}{\xi^{3/2}} \pm \frac{2\nu}{\xi^{1/2}}\right] = 0 \tag{13}$$

Clearly, solutions of Eqn 13 will depend on the value of A. Here, it is convenient to define a dimensionless geometrical group, T, defining the characteristics of a given tape:

$$T = \alpha\sqrt{R/t} \tag{14}$$

Thus, by Eqn 11

$$A = \frac{2}{[3(1-\nu^2)]^{1/4}} \cdot \frac{1}{T} \approx \frac{1.58}{T} \tag{15}$$

to within ±3 % for $0 \leq \nu \leq 0.5$. For a typical commercially available tape, $T = 15.7$ and $A = 0.10$ (for an assumed circular cross-section), see Table 1 below; for other tapes used in finite element analysis in Fig. 4, T lies between 10 and 30 with $0.15 > A > 0.05$.

4 Results

Solutions of Eqn 13 for given values of A may be obtained in different ways.

In general, Eqn 13 may be solved by a routine function in MATLAB [11]. This has been done for six particular values of A in Fig. 4 (solid lines).

We see that values of ξ are modestly larger than unity; which suggests that we might also investigate an approximate solution of Eqn 13 by replacing ξ with $1 + \gamma$, where γ is expected to be a small quantity. Thus using the Binomial Theorem and retaining quadratic terms in γ, Eqn 13 can be re-written

R	t	α [rad]	b	H	R/t	T	A	L^*/b	$T/\sqrt{H/t}$
13	0.125	1.54	20	3.67	104	15.7	0.10	1.16	2.90
10	0.1	$\pi/3$	10.5	1.34	100	10.5	0.15	1.16	2.86
20	0.2	$\pi/2$	31.4	5.86	100	15.7	0.10	1.75	2.90
10	0.1	$2\pi/3$	20.9	5.00	100	20.9	0.076	2.33	2.96
20	0.1	$2\pi/3$	41.9	10.00	200	29.6	0.053	3.29	2.96

TABLE 1: Values of T and A (Eqns 14 and 15) for different tapes. Lengths are measured in mm and $\nu = 0.3$. T and A are dimensionless, and Eqn 21 gives values of L^*/b where L^* is the approximate length of the ploy region. Top line: values for a typical carpenter's tape. Other lines relate to tape results in Fig. 4, obtained by finite element analysis.

$$\gamma^2\left[-3+\frac{A}{16}\left(3\mp 6\nu+15\nu^2\right)\right]+\gamma\left[2+\frac{A}{4}\left(-3\pm 2\nu-3\nu^2\right)\right]+\frac{A}{2}\left(-3\mp 2\nu+\nu^2\right)=0 \tag{16}$$

From Table 1, we observed $A = 0.10$ for a typical carpenter's tape. Substituting into Eqn 16 along with $\nu = 0.3$ and selecting the smaller of its two roots, we obtain $\gamma = 0.108$ for OS behaviour and 0.067 for ES: the hinge radius is either 11% or 7% bigger. The scale of these margins complies with the careful measurements reported in [6]; their difference can be gauged informally by tracing (using a sharp pencil) the tape's cross-section and folded hinge profiles, for example.

For thin tapes in which t/R is typically less than 1/100, the value of A in Eqn 11 will generally be much smaller than unity, see Table 1. The coefficients of Eqn 16 may now be simplified by retaining A only in the constant term, to give

$$-3\gamma^2+2\gamma+\frac{A}{2}\left(-3\mp 2\nu+\nu^2\right)=0 \tag{17}$$

Equation 17 has a lesser root:

$$\gamma=\frac{1}{3}-\frac{1}{3}\left[1-\frac{3A}{2}\left(3\pm 2\nu-\nu^2\right)\right]^{1/2} \tag{18}$$

Hence

$$\xi = \frac{4}{3} - \frac{1}{3}\left[1 - \frac{3A}{2}\left(3 \pm 2\nu - \nu^2\right)\right]^{1/2} \tag{19}$$

This suggests that the expression multiplying A in Eqn 13 need only be evaluated for $\xi = 1$ in the γ calculation.

When A approaches zero (say, tapes with a large value of $\alpha\sqrt{R/t}$):

$$\xi \approx 1 + \frac{A}{4}(3 \pm 2\nu - \nu^2) \tag{20}$$

In Fig. 4 we compare solutions for ξ obtained numerically from Eqn 13 with approximate solutions *via* Eqn 19. In general, Eqn 19 provides a good approximation to the numerical solutions of Eqn 13—at least for the range of variables deployed here. And indeed the various curves are strikingly linear in $(\pm)\ \nu$, as if the term $(3 \pm 2\nu)$ in Eqns 19 and 20 and elsewhere plays a dominant role.

Figure 4 also includes discrete data from a finite element analysis of several tape geometries listed in Table 1 and similar to a standard carpenter's tape. In addition, ν was either 0.2, 0.3 or 0.4 for each tape, and the Young's modulus was set to a nominal value of 131 GPa: its absolute value does not alter the findings, of course.

For these computations we used the commercial package ABAQUS [12] and the same tape-bending formulation using S4R5 elements as in references [6, 8]. Hinges are formed robustly from the buckling-induced bending of straight tapes in both ES and OS using the stabilising parameter set to default values within the static option from ABAQUS; geometrical nonlinearity is active, and the material is linear elastic.

In the computations, the tape must also be long enough to accommodate the natural lengths and shapes of the ploy regions and the hinge during folding. The arc-length of the latter is $r\psi$, and Seffen *et al.* [13] estimate the "characteristic" length, L^*, of the ploy region to be $(1/9) \cdot b^2/\sqrt{Rt}$ for $\nu = 0.3$.

Typical values of L^* have already been given in Table 1, and are several times larger than R because of the "long-wave" nature of the ploy shape assumed in [13]. In particular, when L^* is compared to the width of tape, b, a simple dimensionless ratio is found in terms of T:

$$\frac{L^*}{b} \approx \frac{1}{9} \cdot \frac{b}{\sqrt{Rt}} = \frac{T}{9} \approx \frac{1}{3}\sqrt{\frac{H}{t}} \tag{21}$$

Here the approximate relationship between T and H (the height of cross-section, Fig. 1) has been taken from Table 1.

5 Discussion

The results in Fig. 4 show an almost-linear dependence on the Poisson's ratio ν. This is in contrast to the role of ν in many problems involving elastic plates and shells, where ν often appears weakly, in the expression $(1-\nu^2)^{1/4}$.

The linear dependance of ξ on ν in the present problem is attributable to the spurious edge moments M_y, shown in Fig. 2, which are properly annulled in the boundary layers. These boundary layers are of precisely the same kind as those first proposed by Lamb and Basset in their discussion, as referees, of Love's celebrated shell paper of 1888 [3].

The parameter T turns out to be important in several ways. The size of ξ in general depends reciprocally on T. Furthermore, the approximation of ξ from Eqn 19 becomes more accurate when T gets larger. T depends solely on the initial geometry but the dimensionless ratio, $T/\sqrt{H/t}$, is almost constant whatever the size of cross-section, see Table 1 (and equal to $2\sqrt{2}$ when α is small); and T simply expresses the length of the ploy region relative to the tape width, *c.f.* Eqn 21.

The difference between r and R also affects the size of the external moments required to maintain the folded shape. These moments are approximately equal to $M_x \cdot b$, and Rimrott's result gives a simple expression of $D\alpha(1 \pm \nu)$ using Eqn 3. However, the true value of r reduces χ_x from $1/R$ by up to 15%, for the range of tapes considered here. Therefore, the value of the applied moments reduces by up to 10% (for $\nu = 0.3$), which may prove significant, depending on how the tape is used (*e.g.* in deploying structures [8]).

In this paper we have followed Rimrott [5] in assuming a sharp transition between the hinge and ploy regions. In fact, as may be observed either directly on a hand-held tape or indirectly *via* a finite element assay, there is a more complex transition zone.

It follows that the folded hinge angle is actually slightly smaller than the relative rotation between the far ends of the tape; the shape of the ploy regions thus encroaches on Rimrott's proposed hinge geometry in Fig. 1. This anomaly does not change our calculation of hinge radius r (because it is independent of ψ); but it suggests further study of the true shape of the ploy region. The difference between these two angles is evident when a tape bent (either in ES or OS) is slowly unfolded: close to the end of the process, the arc-length of fold becomes zero just before the tape "snaps" back to fully straight.

Some of our finite element computations were made with artificially high values of ψ, in order to simplify the measurement of the hinge radius r. Indeed, the computational points plotted in Fig. 4 correspond to $\psi = 2\pi$, a possibility that is afforded by finite elements, when "no contact" conditions are specified.

Throughout our analysis we have assumed tacitly that *torsional* behaviour of the tape plays no part in the formation of a localised hinge under increasing bending moments. Anyone who has attempted to bend a length of relaxed, straight tape between two hands will have observed torsional deformation of the tape in the early stages of bend-formation, particularly in ES.

Mansfield [10] studied the onset (and relief) of torsional buckling when the longitudinal curvature remains uniform *i.e.* without the hinge localising. Evidently, there is plenty of scope for further investigation of tape-bending (and -twisting) phenomena.

References

[1] G T Bennett. A new four-piece skew mechanism. *Engineering*, 76:777–778, 1903.

[2] E H Milne. A E H Love: Obituary notices of Fellows of the Royal Society, 1939-1941. 3:466–482, 1941.

[3] C R Calladine. The theory of thin shell structures 1888-1988: Love Centenary Lecture. *Proceedings of the Insititute of Mechanical Engineers*, 202:141–149, 1988.

[4] K A Seffen. *Analysis of Structures Deployed by Tape-Springs.* PhD thesis, University of Cambridge, 1997.

[5] F P J Rimrott. Querschnittsverformung bei torsion offener profile. *Zeitschrift fur Angewandte Mathematik und Mechanik*, 50:775–778, 1970.

[6] K A Seffen. On the behaviour of folded tape-springs. *Journal of Applied Mechanics, Transactions ASME*, 68:369–375, 2000.

[7] C R Calladine. *Theory of Shell Structures*. Cambridge University Press, 1983.

[8] K A Seffen and S Pellegrino. Deployment dynamics of tape-springs. *Proceedings of the Royal Society of London, A*, 455:1003–1048, 1999.

[9] W Wuest. Einige anwendungen der theorie der zylinderschale. *Zeitschrift fur Angewandte Mathematik und Mechanik*, 84:444–454, 1954.

[10] E H Mansfield. Large-deflexion torsion and flexure of initially curved strips. *Proceedings of the Royal Society of London, A*, 334:279–298, 1973.

[11] The Mathworks. *MATLAB, Version 2013b*, 2013.

[12] Hibbitt and Karlsson and Sorensen. *ABAQUS/Standard User's Manual, Version 6.14*, 2014.

[13] K A Seffen, B Wang, and S D Guest. Folded orthotropic tape-springs. *Journal of the Mechanics and Physics of Solids*, 123:138–148, 2019.

Figures

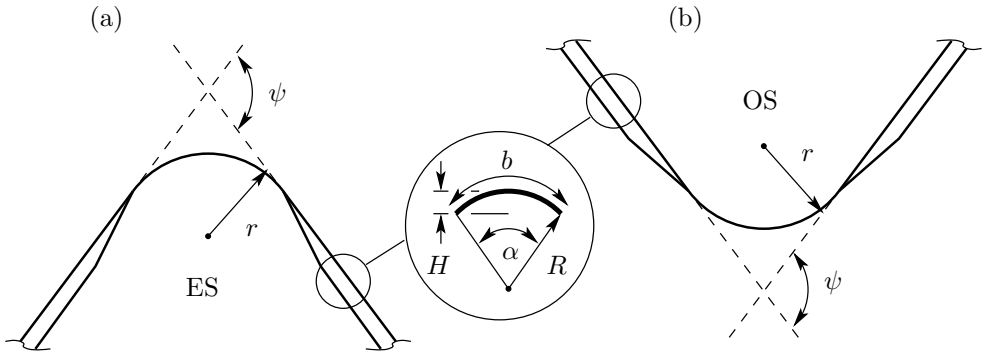

FIGURE 1: A bent carpenter's tape in side-view. (a) Equal-sense (ES) bending and (b) opposite-sense (OS) bending. The initial transverse circular cross-section, inset, has radius R, subtends arc-width $b = R\alpha$, and has height H, equal to $R(1 - \cos\alpha/2)$. The bent fold region subtends arc-length ψ at constant radius r.

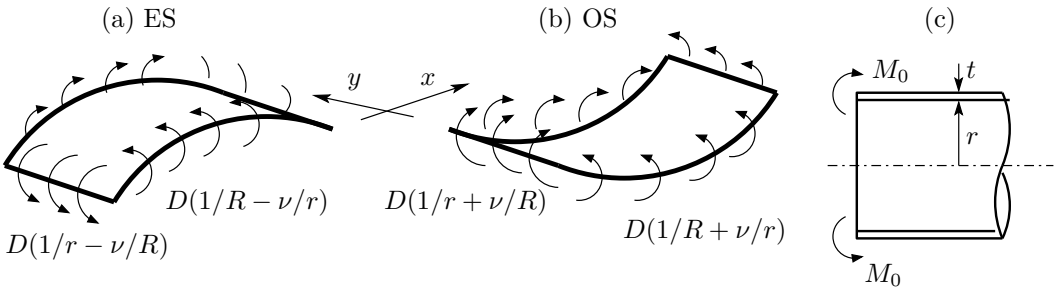

FIGURE 2: Edge moments present in a uniformly curved hinge for (a) ES bending and, (b), OS bending. (c) Equivalent end-loaded cylinder.

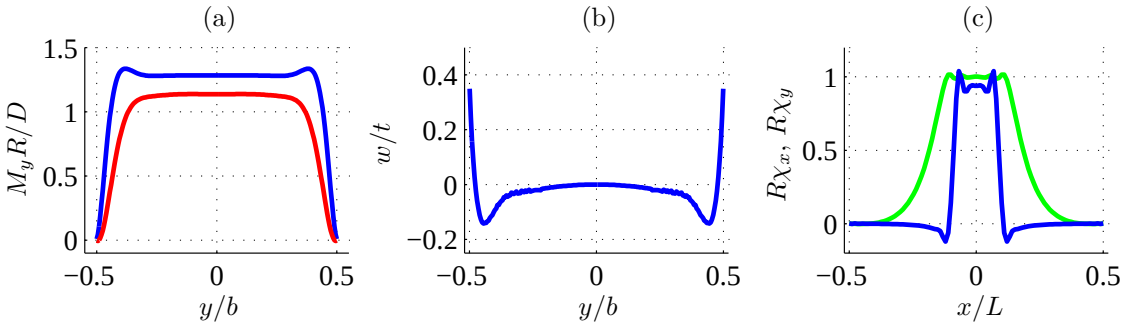

FIGURE 3: Nominal properties of a bent tape (OS). Initial geometry as per Fig. 1 with $E = 131$ GPa, $\nu = 0.3$, $R = 10$ mm, $t = 0.1$ mm and $\alpha = 2\pi/3$ radians. (a) Transverse bending moment, M_y, across the hinge width at two locations: the hinge centre (blue) and just beyond the start of the ploy region (red). (b) Displaced cross-section at the hinge centre: w is the outwards (radial) displacement with respect to the cylindrical surface, resulting in anticlastic curvatures along both edges. (c) Curvature changes along the centre-line (midway between the long edges); χ_x (longitudinal, blue), χ_y (transverse, green). The extent of each ploy region is evinced by χ_y rising from zero to its steady fold value. The length of tape is L, equal to 200 mm, and $\psi = \pi$ radians.

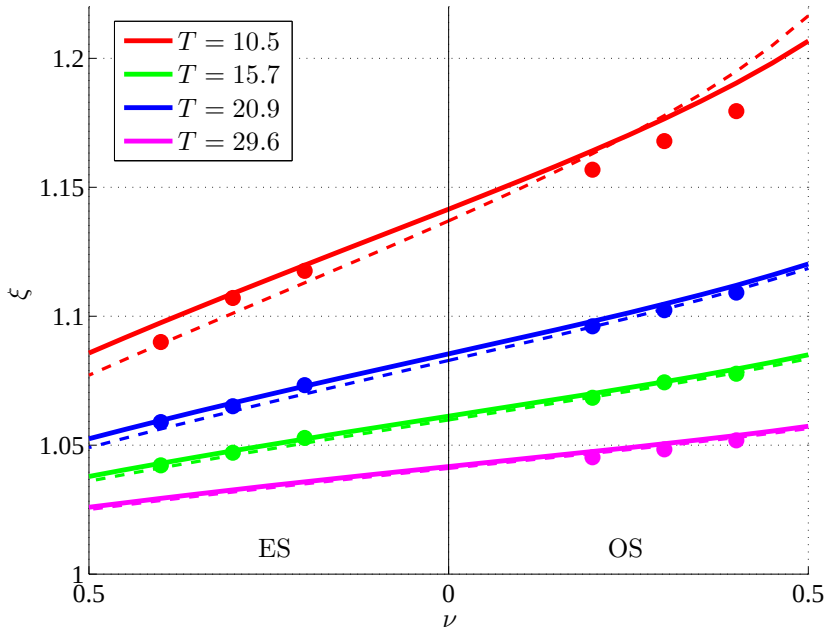

FIGURE 4: Direct numerical solution of Eqn 13 (solid lines) for ES and OS bending. The scales of ν extend to the left for ES and to the right for OS—in accordance with the $\pm\nu$ terms in the various expressions. Dashed lines are ξ from Eqn 19 and solid dots are taken from finite element data according to the geometries in Table 1.